



1 **Landsat and Sentinel-derived glacial lake dataset in the**
2 **China-Pakistan Economic Corridor from 1990 to 2020**

3

4 Muchu Lesi¹, Yong Nie^{1,*}, Dan H. Shugar², Jida Wang³, Qian Deng^{1,4}, Huayong Chen¹

5 ¹Institute of Mountain Hazards and Environment, Chinese Academy of Sciences, Chengdu,
6 China.

7 ²Water, Sediment, Hazards, and Earth-surface Dynamics (waterSHED) Lab, Department of
8 Geoscience, University of Calgary, Alberta, T2N 1N4, Canada

9 ³Department of Geography and Geospatial Sciences, Kansas State University, Manhattan,
10 Kansas 66506, USA

11 ⁴University of Chinese Academy of Sciences, Beijing 100190, China

12

13

14

15

16 *Corresponding author, nieyong@imde.ac.cn

17

18



19 **Abstract.** The China-Pakistan Economic Corridor (CPEC) is one of flagship projects of the
20 One Belt One Road Initiative, which faces threats from mountain disasters in the high altitude
21 region, such as glacial lake outburst floods (GLOFs). An up-to-date high-quality glacial lake
22 dataset with critical parameters (e.g. lake types), which is fundamental to flood risk
23 assessments and predicting glacier-lake evolutions, is still largely absent for the entire CPEC.
24 This study describes a glacial lake dataset in 2020 for CPEC at 10-30 m resolution, which
25 was produced from both Landsat and Sentinel optical images as well as glacial lake
26 inventories in 1990 and 2000 from Landsat observation, using an advanced object-oriented
27 mapping method associated with rigorous visual inspection workflows. The results show that
28 Landsat derived 2234 glacial lakes in 2020, covering a total area of $86.31 \pm 14.98 \text{ km}^2$ with a
29 minimum mapping unit of 5 pixels (4500 m^2), whereas Sentinel derived 7560 glacial lakes in
30 2020 with a total area of $103.70 \pm 8.45 \text{ km}^2$ with a minimum mapping unit of 5 pixels (500 m^2).
31 The discrepancy implies that there is a significant quantity of small glacier lakes not
32 recognized in existing glacial lake inventories and a more thorough inclusion of them require
33 future efforts using higher resolution data. The total number and area of glacial lakes from
34 consistent 30 m resolution Landsat images remain relatively stable despite a slight increase
35 from 1990 to 2020. A range of critical attributes have been generated in the dataset, including
36 lake types of two classification systems and mapping uncertainty estimated by an improved
37 equation. This comprehensive glacial lake dataset has potentials to be widely applied in
38 studies on glacial lake-related hazards and glacier-lake interactions, and is freely available at
39 <https://doi.org/10.12380/Glaci.msdc.000001> (Lesi et al., 2022).

40 **1 Introduction**

41 Glaciers in High-mountain Asia (HMA) play a crucial role in regulating climate, supporting
42 ecosystems, modulating the release of freshwater into rivers, and sustaining municipal water
43 supplies (Wang et al., 2019; Viviroli et al., 2020), agricultural irrigation, and hydropower
44 generation (Pritchard, 2019; Nie et al., 2021). Most HMA glaciers are losing mass in the
45 context of climate change (Brun et al., 2017; Shean et al., 2020; Bhattacharya et al., 2021;
46 Maurer et al., 2019), therefore, unsustainable glacier melt is reducing the hydrological role of
47 glaciers and impacting downstream ecosystem services, agriculture, hydropower and other
48 socioeconomic values (Nie et al., 2021). The present and future glacier changes also alter the
49 frequency and intensity of glacier-related hazards, such as glacier lake outburst floods
50 (GLOFs) (Nie et al., 2018; Zheng et al., 2021; Rounce et al., 2020), and rock and ice
51 avalanches (Shugar et al., 2021). The increasing frequency of GLOFs has been observed in
52 the Karakoram and Himalaya (Nie et al., 2021), and the increasing risk of GLOFs is
53 threatening existing and planned infrastructures in the mountain ranges, such as hydropower
54 plants, railways, and highways.

55 A large number of major infrastructure construction projects for the One Belt One Road
56 Initiative (BRI) play a fundamental role in strengthening the interconnection of infrastructure
57 between countries and promoting international trade and investment (Battamo et al., 2021; Li
58 et al., 2021). Taking the Karakoram Highway for example, it is a unique land route to link



59 China and Pakistan. The China-Pakistan Economic Corridor (CPEC) is one of the BRI
60 flagship projects, originating from Kashgar of the Xinjiang Uygur Autonomous region, China
61 and extending to Gwadar Port, Pakistan (Ullah et al., 2019; Yao et al., 2020). The northern
62 section of the CPEC passes through Pamir, Karakoram, Hindu Kush and Himalaya mountains
63 where glacier-related hazards such as GLOFs are frequent and severe (Hewitt, 2014; Bhambri
64 et al., 2019), threatening the existing, under-construction and planned infrastructure projects.
65 Understanding the risk posed by GLOFs is a critical step to disaster prevention for
66 infrastructures across the CPEC (Figure 1).

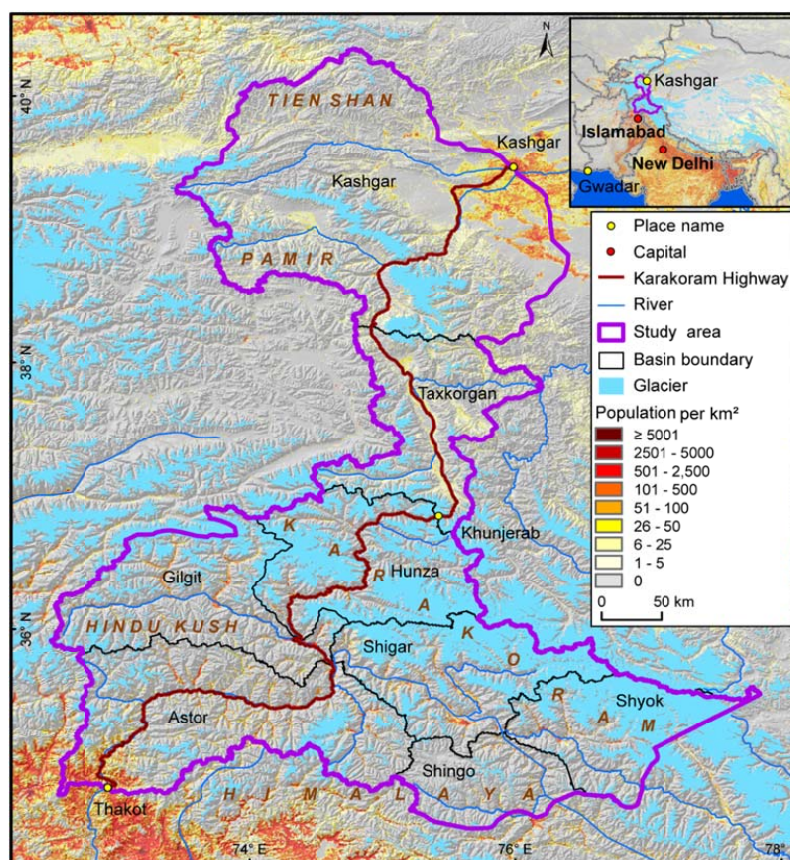
67 Glacial lake inventories with a range of attributes benefit risk assessment and disaster
68 reduction related to GLOFs, and contribute to predicting glacier-lake evolution under climate
69 change (Nie et al., 2017; Brun et al., 2019; Liu et al., 2020; Maurer et al., 2019). Remote
70 sensing is the most viable way to map glacial lakes and detect their spatio-temporal changes
71 in the high-elevation zones where in situ accessibility is extremely low (Huggel et al., 2002;
72 Quincey et al., 2007). Studies in glacial lake inventories using satellite observations have
73 been heavily conducted at regional scales recently, such as in the Tibetan Plateau (Zhang et
74 al., 2015), the Himalaya (Gardelle et al., 2011; Nie et al., 2017), the HMA (Chen et al., 2021;
75 Wang et al., 2020), the Tien Shan (Wang et al., 2013) and the northern Pakistan (Ashraf et al.,
76 2017). However, the latest glacial lake mapping in 2020 is still absent along the CPEC.
77 Among existing studies, Landsat archival images are the most widely used due to their
78 multi-decadal record of earth surface observations, reasonably high spatial resolution (30 m),
79 and publicly available distribution (Roy et al., 2014). Freely available Sentinel-2 satellite
80 images show a better potential than Landsat in glacial lake mapping and inventories due to
81 their higher spatial resolution (10 m) and a global coverage, but have only been available
82 since late 2015 (Williamson et al., 2018; Paul et al., 2020). Glacial lake inventories using
83 Sentinel images are relatively scarce at regional scales, and studies of the latest glacial lake
84 mapping as well as comparisons of glacial lake datasets derived from Sentinel and Landsat
85 observations are still lacking.

86 Discrepancies between various glacial lake inventories (Zhang et al., 2015; Shugar et al.,
87 2020; Chen et al., 2021; Wang et al., 2020) result from differences in mapping methods,
88 minimum mapping units, definition of glacial lakes, time periods, data sources and other
89 factors. For example, manual vectorization method was widely adopted at the earlier stage for
90 its high accuracy. However, it is time-consuming associated with high labor intensity and is
91 only practical at regional scales (Zhang et al., 2015; Wang et al., 2020). Automated and
92 semi-automated lake mapping methods, such as band ratio and object-oriented classification
93 (Gardelle et al., 2011; Zhang et al., 2018; Nie et al., 2017), have been developed to improve
94 the efficiency of glacial lake inventories, although artificial modification is unavoidable to
95 assure the quality of lake data impacted by cloud cover in optical images, mountain shadows,
96 seasonal snow cover and frozen lake surfaces (Sheng et al., 2016; Wang et al., 2017; Wang et
97 al., 2018). Type classification of glacial lakes provides a crucial attribute for glacier-lake
98 interactions and risk assessment (Emmer and Cuřin, 2021). Glacier lakes in currently
99 available datasets have been traditionally categorized by their spatial relationship with
100 upstream glaciers (Gardelle et al., 2011; Chen et al., 2021; Wang et al., 2020), and
101 classification attributes considering the formation mechanism and the properties of dams are
102 rare or incomplete in the CPEC (Li et al., 2021; Yao et al., 2018). Therefore, an up-to-date



103 glacial lake dataset with critical, quality-assured parameters (e.g. lake types) is necessary.
104 This study aims to (1) employ both Landsat 8 and Sentinel-2 images to create an up-to-date
105 glacial lake dataset in the CPEC to accurately document its detailed lake distribution in 2020;
106 (2) reveal glacial lake changes and the spatial heterogeneity across mountains and basins in
107 the CPEC using consistent 30-m Landsat images at three time periods (1990, 2000 and 2020);
108 and (3) share the glacial lake inventories with a range of critical attributes to benefit
109 hazardous risk assessment of GLOFs and glacio-hydrological modeling in the HMA.

110 2 Study area



111
112 **Figure 1.** Location of the study area and distribution of glaciers, mountains, basins and population.
113

114 The study area (**Figure 1**) covers all the drainage basins along Karakoram Highway starting
115 from Kashgar and ending at Thakot, with a total area of $\sim 125,000 \text{ km}^2$. The upper Indus
116 basins beyond the Pakistani-administrated border are excluded in this study due to little
117 impact of GLOFs there on CPEC infrastructures. The entire study area is divided into eight
118 sub-basins, covering most of the Karakoram with the highest altitude up to 8611 m, western
119 Himalaya and Tien Shan, eastern Hindu Kush and Pamir mountains. The 9710 glaciers in the
120 study area cover a total area of $17,447 \text{ km}^2$ and nearly 60% of glaciers are distributed in the



121 Karakoram (5818 glaciers with a total area of 14,067.52 km²) (RGI Consortium, 2017). Most
122 glaciers in the western Himalaya and eastern Hindu Kush are losing mass in the context of
123 climate change (Kääb et al., 2012; Yao et al., 2012; Shean et al., 2020; Brun et al., 2017;
124 Hugonnet et al., 2021), whereas the glaciers in the eastern Karakoram and Pamir have shown
125 unusually little changes, including unchanged, retreated, advanced and surged glaciers (Nie et
126 al., 2021; Brun et al., 2017; Shean et al., 2020; Kääb et al., 2012; Hewitt, 2005; Bolch et al.,
127 2017). The spatially heterogeneous distribution and changes of glaciers are primarily
128 explained as a result of differences in the dominant precipitation-bearing atmospheric
129 circulation patterns that include the winter westerlies the Indian summer monsoon, their
130 changing trends and their interactions with local extreme topography (Azam et al., 2021; Nie
131 et al., 2021; Yao et al., 2012).

132 **3 Data sources**

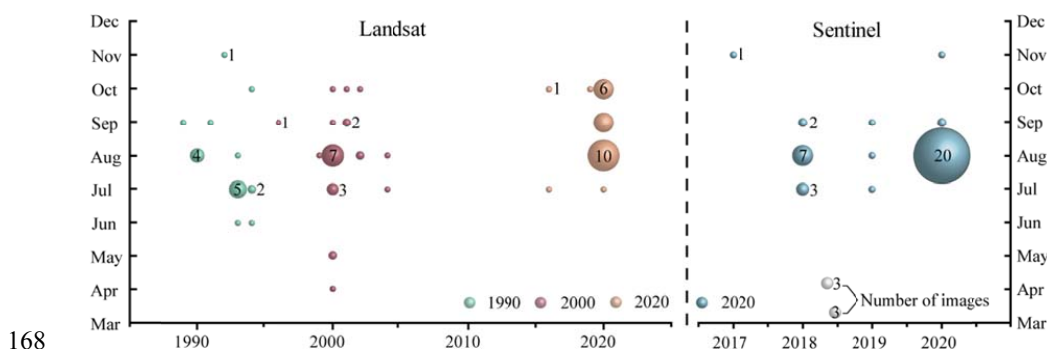
133 Both Landsat and Sentinel images have been employed to map glacial lakes between 1990
134 and 2020 in the CPEC (Figure 2). A total number of 98 Landsat Thematic Mapper (TM),
135 Thematic Mapper Plus (ETM+) and Landsat 8 Operational Land Imager (OLI) images with a
136 consistent spatial resolution of 30 m were downloaded from the United States Geological
137 Survey Global Visualization Viewer (GloVis, <https://glovis.usgs.gov/app/>) to be used to create
138 glacial lake inventories in 1990, 2000 and 2020. High-quality Landsat images around 2010
139 are insufficient to cover the entire study area, so we had to give up glacial lake mapping in
140 2010 as a result of Landsat 7's scan-line corrector errors and significant cloud covers. In
141 addition, 40 Sentinel-2 images were downloaded from Copernicus Open Access Hub
142 (<https://scihub.copernicus.eu/>) to produce the 10-m resolution glacial lake inventory in 2020.

143 Cloud and snow covers heavily affect the usability of optical satellite images (Wulder et
144 al., 2019) and their availability in the entire study area, so we took advantage of the images
145 acquired before and after each of the baseline years 1990, 2000 and 2020 to construct the
146 glacial lake inventories. To minimize the impact of intra-annual changes of glacial lakes,
147 most of used images (85% for Sentinel and 82% for Landsat) were acquired from August to
148 October in the given baseline year with cloud coverage of <20% for each image. For some
149 specific scenes where cloud cover exceeded the threshold of 20%, we selected more than one
150 image to remedy the effect of cloud contamination (Nie et al., 2010; Nie et al., 2017; Jiang et
151 al., 2018).

152 Other datasets used include the Randolph Glacier Inventory version 6.0 (Pfeffer et al.,
153 2014; RGI Consortium, 2017) and the Glacier Area Mapping for Discharge from the Asian
154 Mountains (GAMDAM) glacier inventory (Sakai, 2019). These two glacier datasets were
155 used to determine glacial lake attributes. The Shuttle Radar Topography Mission Digital
156 Elevation Model (SRTM DEM) at a 1-arc second (30 m) resolution (Jarvis et al., 2008) was
157 employed to extract the altitudinal characteristics of the glacial lakes. The absolute vertical
158 accuracy of the SRTM DEM is 16 m (90%) (Farr et al., 2007; Rabus et al., 2003). We also
159 applied other published glacial lake datasets for comparative analysis. They include the
160 glacial lake inventories of HMA in 1990 and 2018 downloaded from
161 <http://doi.org/10.12072/casnw.064.2019.db> (Wang et al., 2020), the Third Pole region in 1990,
162 2000 and 2010 publicly shared at <http://en.tpdatabase.cn/> (Zhang et al., 2015), the Tibet
163 Plateau from 2008 to 2017 accessed at <https://doi.org/10.5281/zenodo.3700282> (Chen et al.,



164 2021), and the entire world in 1990, 2000 and 2015 provided at https://nsidc.org/data/HMA_
165 [GLI/versions/1](https://nsidc.org/data/HMA_GLI/versions/1) (Shugar et al., 2020). In addition, field survey data collected between 2017
166 and 2018 were also used to assist in lake mapping and glacial lake type classification.
167



168
169 **Figure 2.** Acquisition years and months of Landsat and Sentinel images selected for glacial lake
170 inventories. The bubble size indicates the available image number.

171 4 Glacial lake inventory methods

172 4.1 Definition of glacial lakes

173 We consider a glacial lake as one that formed as a result of modern or ancient glaciation.
174 Contemporary glacial lakes are easily recognized using a combination of glacier inventories
175 and remote sensing images. Ancient glacial lakes can be identified from periglacial
176 geomorphological characteristics, including moraine remnants and U-shaped valleys that are
177 discernible from satellite observations (Post and Mayo, 1971; Nie et al., 2018; Martín et al.,
178 2021; Westoby et al., 2014). Landslide-dammed lakes (Chen et al., 2017) in the periglacial
179 environment were excluded in our inventories because of their irrelevance to glaciation. We
180 abandoned the definition that considers all lakes surrounding a specific buffering distance of
181 other glaciers also as glacier lakes, although this definition has been widely used in previous
182 studies assuming glacial meltwater as the main water supply (Zhang et al., 2015; Wang et al.,
183 2020). This is because the contribution of glacial meltwater to the lake supply is arduous to
184 be quantified without an accurate modeling of the cryosphere-hydrological processes (Lutz et
185 al., 2014). All glacial lakes in the study area were mapped according to our definition without
186 any distance limit between lakes and glaciers. We were able to implement this definition by
187 carefully leveraging the spectral properties of glacial lakes and the periglacial
188 geomorphological features that are often evident in remote sensing images (see more in
189 sections 4.3 and 4.4).

190 4.2 Interactive lake mapping

191 A human-interactive and semi-automated lake mapping method (Wang et al., 2014; Nie et al.,
192 2017; Nie et al., 2020) was adopted to accurately extract glacial lake extents using Landsat
193 and Sentinel-2 images, based on the Normalized Difference Water Index (NDWI) (Mcfeeters,



194 1996). The NDWI uses the green and near infrared bands and is calculated by the following
195 equation:

$$196 \quad NDWI = \frac{Band_{Green} - Band_{NIR}}{Band_{Green} + Band_{NIR}} \quad (1)$$

197 where the green band and near infrared band were provided by both Landsat and Sentinel
198 multispectral images.

199 Specifically, the method automatically generated the histogram of NDWI in each
200 user-defined region of interest. The NDWI threshold that separates lake surface from land
201 was interactively determined by screening the NDWI histogram against the lake region in the
202 imagery (Nie et al., 2020; Wang et al., 2012). This way, the determined NDWI threshold can
203 be well-tuned to adapt various spectral conditions of the studied glacier lakes. The raster lake
204 extents segmented by the thresholds were then converted to vector polygons. We first
205 completed the glacial lake inventory in 2020 using this interactive mapping method, and the
206 2020 inventory was then used as a reference to facilitate the lake mapping for other periods.

207 The minimum mapping unit (MMU) was set to 5 pixels for both Landsat (0.0045 km²) and
208 Sentinel-2 images (0.0005 km²) in this study. MMU determines the total number and area of
209 glacial lakes in the dataset, and varies in the previous studies, such as 3 pixels (Zhang et al.,
210 2015), 9 pixels (Chen et al., 2021), or 55 pixels (Shugar et al., 2020) for Landsat images for
211 various objectives and spatial scales. While a smaller threshold leads to a large quantity of
212 lakes mapped, it also generates larger mapping noises or uncertainties. Considering this
213 signal-noise balance and our focus on identifying prominent glacier lake dynamics in the
214 study area, we opted to use 5 pixels as the minimum mapping unit for both Landsat and
215 Sentinel-2 images.

216 Several procedures were taken to assure the quality assurance and quality control for lake
217 mapping, including 1) visual inspection and modification for each lake based on Landsat,
218 Sentinel-2 and Google Earth high-resolution images overlaying preliminarily lake boundary
219 extraction at the given time period; 2) time series check for Landsat-derived glacial lake
220 datasets from 1990 and 2020, and cross-check between Landsat and Sentinel-2-derived lake
221 dataset in 2020 to reduce errors of omission and commission; 3) topological validation of
222 glacial lake mapping, such as repeated removal, elimination of small sliver polygons; and 4)
223 logical check for lake types between two classification systems of glacial lakes. False lake
224 extents resulting from cloud or snow cover, lake ice, and topographic shadows (Nie et al.,
225 2020; Nie et al., 2017) and were modified using alternative images acquired in adjacent years.
226 Those procedures were time-consuming, but helped to minimize the effect of cloud and snow
227 covers, lake mapping errors, and to maximize the quality of the produced lake product and
228 the derived glacial lake changes.

229 4.3 Classification of glacial lakes

230 Two glacial lake classification systems (GLCS) have been established based on relationship
231 of interaction between glacial lakes and glaciers as well as lake formation mechanism and
232 dam material properties. In the first GLCS (GLCS1), glacial lakes were classified into four
233 types based on their spatial relationship to upstream glaciers: supraglacial, proglacial,
234 unconnected-glacier-fed lakes, and non-glacier-fed lakes according to Gardelle et al. (2011).
235 Alternatively, combining the formation mechanism of glacial lakes and the properties of



236 natural dam features, glacial lakes were classified into five categories (herein named GLCS2)
 237 modified from Yao's classification system (2018): supraglacial, end-moraine dammed,
 238 lateral-moraine dammed, glacial erosion lakes and ice-blocked lakes. Characterization and
 239 examples for each type are provided in **Table 1** and **Table 2**. Individual glacial lakes were
 240 categorized to the specific types for each GLCS according to available glacier inventory data,
 241 geomorphological and spectral characteristics interpreted from Landsat, Sentinel and Google
 242 Earth images. The synergy of these two GLCSs is beneficial to predicting glacier-lake
 243 evolutions and providing fundamental data for glacial lake disaster risk assessment.

244
 245 **Table 1.** Classification system of glacial lake types according to the relationship between glacial lakes and
 246 glaciers (© Google Earth 2019).

Lake types	Characteristics	Landsat	Sentinel	Google earth
Supraglacial	Lakes formed on the surface of glaciers, generally dammed by ice and thin debris. Case location: 35°43'49.74" N 76°13'53.88" E			
Proglacial	Lakes dammed by moraine, ice or bedrock, supplied by glacial meltwater and connected with glaciers. Case location: 39°09'32.40" N 73°43'12.00" E			
Unconnected-glacier-fed	Lakes currently supplied by upstream glacial meltwater but disconnected with glaciers. Case location: 35°47'60.00" N 72°55'15.60" E			
Non-glacier-fed	Lakes formed by glaciology, dammed by moraine or bed rock, and currently not supplied by glacial meltwater. Case location: 34°50'39.99" N 74°48'29.31" E			

247



248 **Table 2.** Classification system of glacial lake types according to the formation mechanism of glacial lakes
 249 and dam material properties (© Google Earth 2019).

Lake types	Characteristics	Landsat	Sentinel	Google earth
Supraglacial	Lakes formed on the surface of glaciers, generally dammed by ice and thin debris. Case location: 36°46'7.39" N 74°20'7.59" E			
End-moraine-dammed	Lakes formed behind moraines as a result of glacier retreat and downwasting. Case location: 35°42'50.40" N 73°09'57.60" E			
Lateral moraine-dammed	Lakes formed behind lateral glacial moraine ridges and dammed by debris, different from ice-blocked glacial lake. Case location: 38°28'45.62" N 75°20'52.30" E			
Glacial erosion	Lakes formed in depressions created by glacial over-deepening. Bedrock dam dominates, partially superimposed by top moraine in rugged terrain. Dams are unclear in the satellite images. Case location: 35°55'55.56" N 73°38'20.13" E			
Ice-blocked	Lakes formed behind glaciers, dammed by glacier ices (partially covered by debris on the top). Case location: 35°28'31.32" N 77°30'46.81" E			

250

251 **4.4 Attributes of glacial lake data**

252 A total of 17 attribute fields were input into our glacial lake datasets (**Table 3**). They include
 253 lake location (longitude and latitude), lake elevation (centroid elevation), orbital number of
 254 the image source, image acquisition date, lake area, lake perimeter, lake types of the two
 255 GLCSs, mapping uncertainty, and the country, sub-basin, and mountain range associated with
 256 the lake. Amongst the attributes, lake location was calculated based on the centroid of each
 257 glacial lake polygon associated with the DEM, N represents northing and E represents easting.



258 Orbital number of the image source was filled with the corresponding satellite image, with
 259 the codes expressed as “PxxxRxxx” or “Txxxxx”, where P and R indicate the path and row
 260 for Landsat image and T represents the tile of Sentinel image associated with 5 digits code of
 261 military grid reference system. Area and perimeter were automatically calculated based on
 262 glacial lake extents. Lake types were attributed using the characterization and interpretation
 263 marks described in Section 4.3. Mapping uncertainty was estimated using our modified
 264 equation which will be introduced in section 4.5 and supplementary tutorial. Located country,
 265 sub-basin and mountain range of each glacial lake was identified by overlapping the
 266 geographic boundaries of countries, basins and mountain ranges.
 267 **Table 3.** Classification system of glacial lake types according to the formation mechanism of glacial lakes
 268 and dam material properties.

Field Name	Type	Description	Note
FID or OBJECTID	Object ID	Unique code of glacial lake	Number
Shape	Geometry	Feature type of glacial lake	Polygon
Latitude	String	Latitude of the centroid of glacial lake polygon	Degree minute second
Longitude	String	Longitude of the centroid of glacial lake polygon	Degree minute second
Elevation	Double	Altitude of the centroid of glacial lake polygon	Unit: meter above sea level
IMGSOURCE	String	Path and row numbers for Landsat image based on World Reference System 2 or Tile number for Sentinel image based on military grid reference system	PxxxRxxx or Txxxxx
ACQDATE	String	Acquisition date of source image	YYYYMMDD
GLCS1	String	The first classification system of glacial lakes based on relationship of interaction between glacial lakes and glaciers	Supraglacial, Proglacial, Unconnected-glacier-fed, None-glacier-fed
GLCS2	String	The second classification system of glacial lakes based on lake formation mechanism and dam material properties	Supraglacial, End-moraine-dammed, Lateral-moraine-dammed, Glacial erosion and



Field Name	Type	Description	Note
			Ice-blocked
Basin	String	Basin name where glacial lake locates in	
Mountains	String	Mountain name where glacial lake locates in	
Country	String	Country name where glacial lake locates in	
Perimeter	Double	Perimeter of glacial lake boundary	Unit: meter
Area	Double	Area of glacial lake coverage	Unit: square meter
Uncertainty	Double	Uncertainty of glacial lake mapping estimated based on modified Hanshaw's equation (2014).	Unit: square meter
Operator	String	Operator of glacial lake dataset	Muchu, Lesi
Examiner	String	Examiner of glacial lake dataset	Yong, Nie

269

270 4.5 Improved uncertainty estimating method

271 We modified Hanshaw's (2014) equation that had been used to calculate lake-area mapping
 272 uncertainty. Lake perimeter and displacement error are widely used to estimate the
 273 uncertainty of glacier and lake mapping from satellite observation. Hanshaw and Bookhagen
 274 (2014) proposed an equation to calculate the error of area measurement by the number of
 275 edge pixels of the lake boundary multiplied by half of a single pixel area. The number of edge
 276 pixels is simply calculated by the perimeter divided by the grid size. The equation is
 277 expressed as below:

$$278 \quad \text{Error}(1\sigma) = \frac{P}{G} \times 0.6872 \times \frac{G^2}{2} \quad (2)$$

$$279 \quad D = \frac{\text{Error}(1\sigma)}{A} \times 100\% \quad (3)$$

280 Where G is the cell size of the remote sensing imagery (10 m for Sentinel-2 image and 30 m
 281 for Landsat image). P is the perimeter of individual glacial lake (m), and the revised
 282 coefficient of 0.6872 was chosen assuming that area measurement errors follow a Gaussian
 283 distribution. Relative error (D) was calculated by equation 3, in which A is the area of an
 284 individual glacial lake.

285 In the original equation 2, the number of edge pixels varies by the shape of lake and is
 286 indicated by $\frac{P}{G}$. However, the pixels in the corner are double counted (Figure 3). The total
 287 number of repeatedly calculated edge pixels equals the number of inner nodes. Therefore, we
 288 adjusted the calculation of the actual number of edge pixels as the maximum of edge pixels ($\frac{P}{G}$)
 289 subtracting the number of inner nodes. Accordingly, the equation of uncertainty estimation



290 for lake mapping is modified as below:

$$291 \quad \text{Error}(1\sigma) = \left(\frac{p}{G} - N_{inner}\right) \times 0.6872 \times \frac{G^2}{2} \quad (4)$$

292 Where N_{inner} is the number of inner nodes (inflection points) of each lake. The modified
 293 equation is also suitable for lakes with islands (as illustrated in Figure 3b).

294 For polygons without islands (Figure S3a), use the following equation:

$$295 \quad N_{inner} = \left(\frac{N_{Total}-4-1}{2}\right) \quad (5)$$

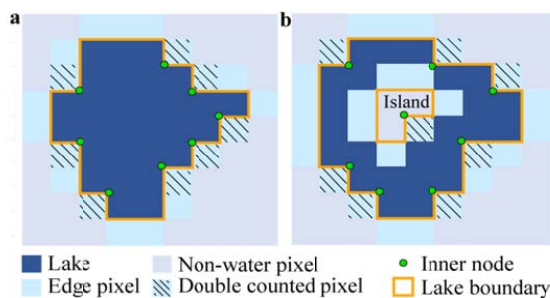
296 N_{Total} is the total number of nodes, including both the outer and inner. N_{Total} were
 297 calculated by the “Field Calculator” in ArcGIS, in some cases, it is necessary to remove the
 298 redundant nodes before calculating the total number of nodes (See the Supplement for more
 299 details). An inner node is a polygon vertex where the interior angle surrounding it is greater
 300 than 180 degrees. An outer node is the opposite of the inner node, where the interior angle is
 301 less than 180 degrees. We found that the outer nodes are usually four more than the inner
 302 nodes in our glacial lake dataset. The total nodes in ArcGIS contain one overlapping node to
 303 close the polygon, meaning the endpoint is also the startpoint. This extra count was deleted in
 304 the calculation (equation 5).

305 For polygons with island (Figure S3b) use the following equation:

$$306 \quad N_{inner} = \left(\frac{N_{Total}-(N_{island}+1)\times 5}{2}\right) \quad (6)$$

307 N_{island} is the number of islands within each polygon. A calculation method of N_{island} is
 308 given in the Supplement.

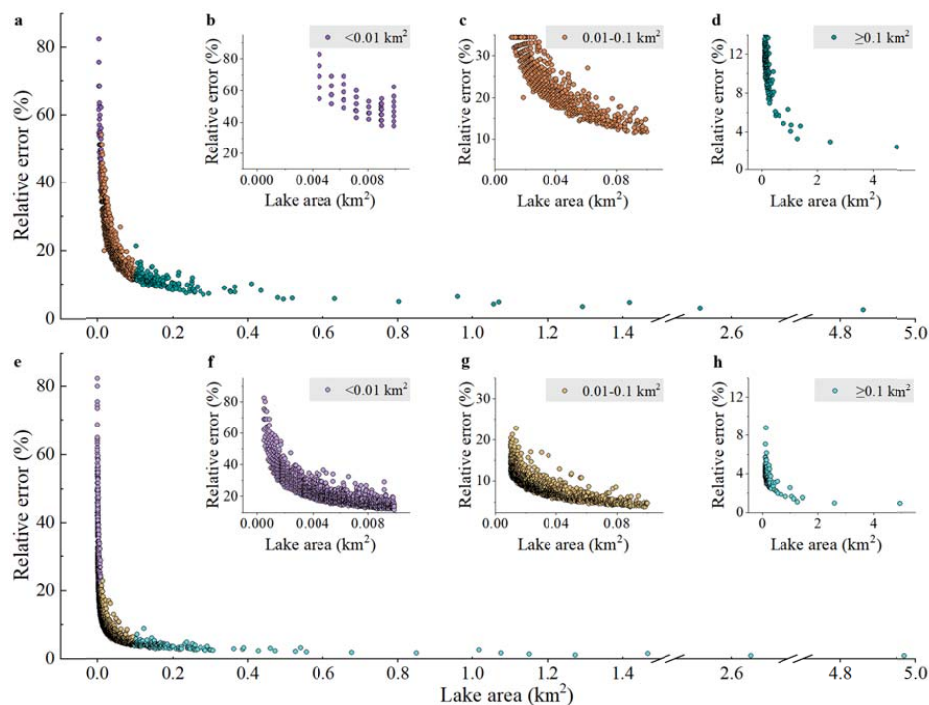
309



310

311 **Figure 3.** Sketch of estimating the actual edge pixels for uncertainty calculation of individual glacial lake

312 (with and without islands).



313

314 **Figure 4.** Relationships between individual lake size and its estimated relative error for glacial lakes of all
315 or specific size ranges in study area. Error estimation is based on the modified equation and lake data
316 extracted from Landsat (a-d) and Sentinel images (e-h).

317

318 The uncertainty estimated from our improved equation shows that the relative error of
319 individual glacial lake decreases when lake size increases or cell size of remote sensing
320 images reduces (Lyons et al., 2013) (Figure 4). Total area error of glacial lakes in study area
321 is approximate $\pm 14.98 \text{ km}^2$ and $\pm 8.45 \text{ km}^2$ in 2020 for Landsat and Sentinel images,
322 respectively, and the average relative error is $\pm 17.36\%$ and $\pm 8.15\%$. Generally, small lakes
323 have greater relative errors. For example, the mean relative error is 35.38% for Landsat
324 derived glacial lakes between 0.0045 and 0.1 km^2 and 10.63% for glacial lakes greater than
325 0.1 km^2 . The mean area error of Sentinel-derived glacial lakes is almost one sixth of that
326 extracted from Landsat images for glacial lakes of all or specific size group.

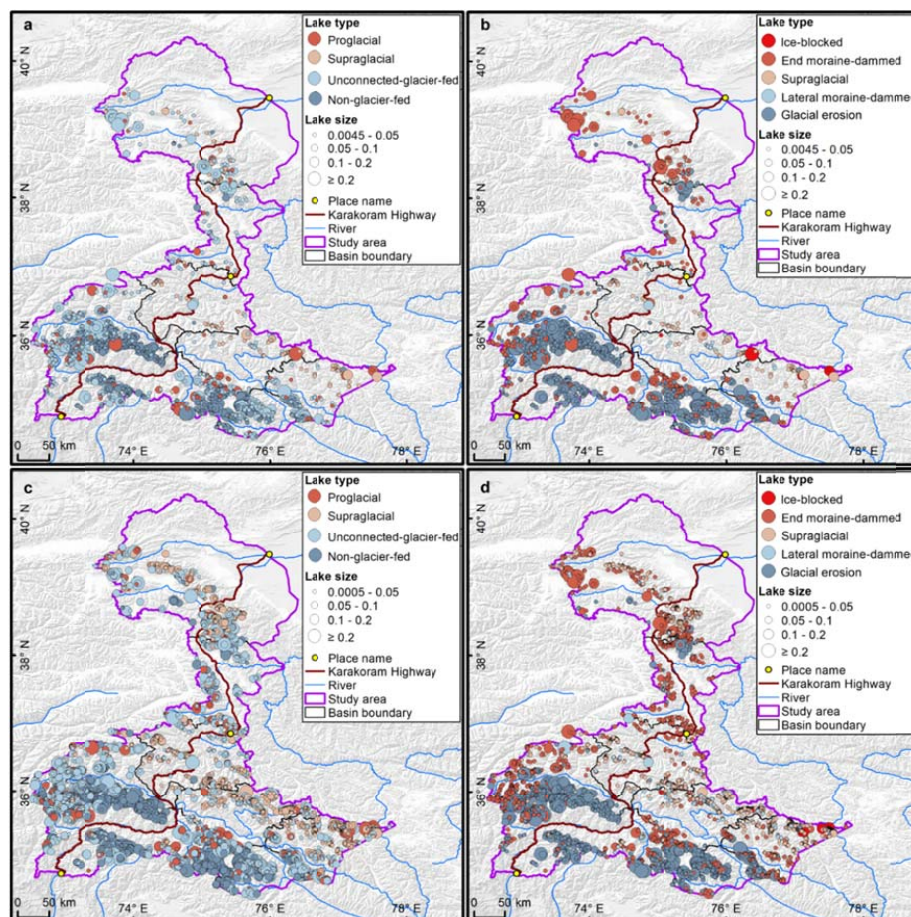
327 5 Results

328 5.1 Glacier lake distribution and changes observed from Landsat

329 We mapped 2,234 glacial lakes for 2020 across the studied CPEC from Landsat-8 images,
330 with a total area of $86.31 \pm 14.98 \text{ km}^2$ (Figure 5a and b). The majority of these glacial lakes
331 (1,870 or 83.71%) are smaller than 0.05 km^2 and contribute 36.5% of the total area. 45
332 (2.01%) of the lakes are larger than 0.2 km^2 and contribute 28.8% of the total area (Figure 6).
333 With the increase of lake size, the abundance (count) of glacial lakes consistently decreases
334 but the total lake area first reduces and then increases. Unconnected-glacier-fed lakes are



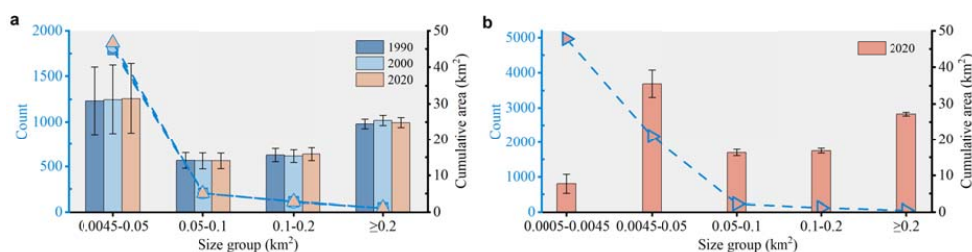
335 dominant in the first classification system, followed by non-glacier-fed lakes (Figure 7)
 336 whereas glacial erosion lakes dominate at both number (1478) and area (57.02 km²) in the
 337 second classification system (Figure 8), followed by end moraine-dammed lakes and
 338 supraglacial lakes. Among the classified lakes, 137 are proglacial lakes and cover an area of
 339 5.56 km², implying a higher mean size of proglacial lakes than supraglacial lakes.
 340 Glacial lakes are spatially heterogeneous among various mountain ranges and basins in the
 341 study area. Himalaya sub-region has the maximum glacier lake count and area across the
 342 entire study area, followed by Hindu Kush. Supraglacial lakes are mainly distributed in the
 343 Karakoram but they cover less area than those in the Pamir. Tien Shan has fewer glacial lakes.
 344 Astor, Gilgit and Shingo basins have the largest percentages of glacier lakes in both number
 345 and area (>17%) (Figure 9a), and each of the other basins contributes less than 10% except
 346 Kashgar basin in area due to several large ancient glacial lakes. Glacial lakes of less than 0.05
 347 km² dominate in number within each basin and the total number decreases as lake size
 348 increases. Small lakes consistently account for the maximum percentage in area except
 349 Kashgar basin as a result of the disproportionately large lakes.



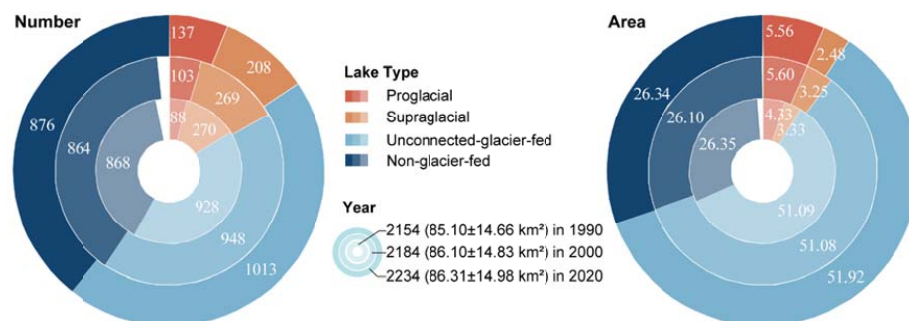
350
 351 **Figure 5.** Distribution of glacial lakes in 2020 extracted from Landsat (a, b) and Sentinel (c, d) images.



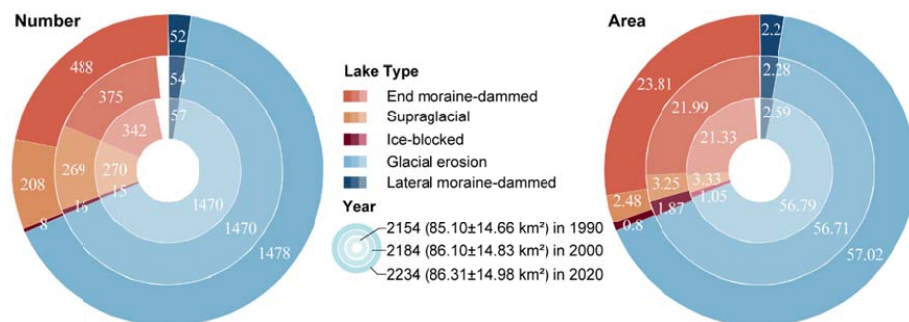
352 Panels a and b are classified by GLCS1, and GLCS2 for sub-graph c and d.
 353



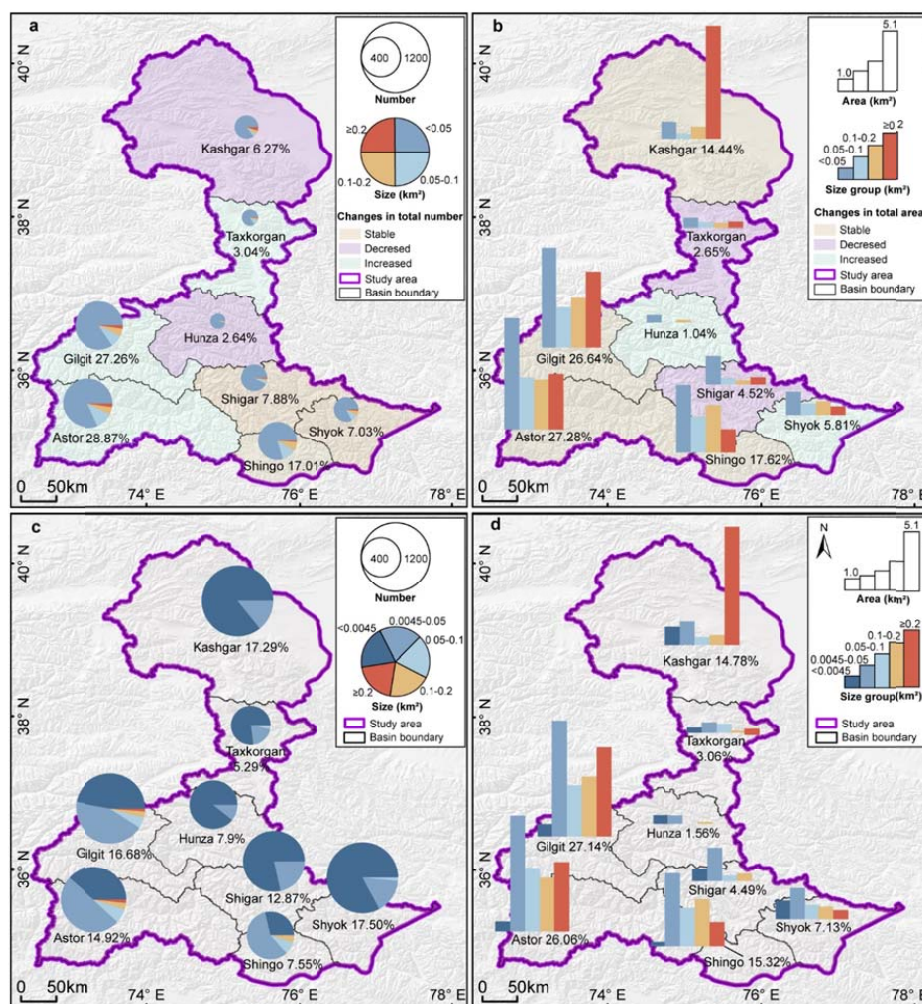
354
 355 **Figure 6.** Statistics of different sizes of glacial lakes in the study area from 1990 to 2020. Panels a and b
 356 were derived from Landsat and Sentinel images, respectively.
 357



358
 359 **Figure 7.** Number and area of different types of glacial lakes classified based on the condition of glacier
 360 supply in the study area. The outermost ring represents glacial lake data in 2020, middle ring for 2000 and
 361 innermost ring for 1990. Lake number and area in 2020 were selected as reference, meaning a concept of
 362 "100 %" for a complete ring. Labeled values are scaled in degrees rather the radius of rings.
 363



364
 365 **Figure 8.** Number and area of different types of glacial lakes classified based on glaciation
 366 and nature of dam in the study area. The outermost ring represents glacial lake data in 2020,
 367 middle ring for 2000 and innermost ring for 1990. Lake number and area in 2020 were
 368 selected as reference, meaning a concept of "100 %" for a complete ring. Labeled values are
 369 scaled in degrees rather the radius of rings.
 370



371
 372 **Figure 9.** Distributions and changes in count and area of glacial lakes. Percent of glacial lakes in number
 373 or area is labeled in each basin. Pie charts present the number of glacial lakes at various size groups
 374 between basins (a and c) and bar charts represent total area of glacial lakes at different size groups in each
 375 basin (b and d). The background colors represent changes in total number and area between 1990 and 2020
 376 based on Landsat derived dataset (a and b) and distribution of Sentinel derived glacial lakes in 2020 among
 377 basins are shown in sub-graphs c and d.

378

379 The total number and area of glacial lakes in the study remain relatively stable with a slight
 380 increase between 1990 and 2020, and the changes in count and area among various types of
 381 glacial lakes vary substantially (Figure 7 and Figure 8). From 1990 to 2020, the total number
 382 of glacial lakes increased by 80 or 3.70%, while the area grew by a less extent (1.21 km² or
 383 1.42%). Small lakes (<0.05 km²) continuously increased in number and area, and contributed
 384 most in the total lake expansion (Figure 6). Lakes in the size group of 0.05-0.1 km² remained
 385 stable. The total area of lakes greater than 0.1 km² consistently increased.



386 In the GLCS1, unconnected-glacier-fed lakes have the largest increase in number, followed
387 by proglacial and non-glacier-fed lakes, whereas supraglacial lakes decreased by 62 in count.
388 Proglacial lakes expanded by 1.24 km² (equaling an increase of 26% in proglacial lakes),
389 contributed one third of the total area increase. Supraglacial lakes decreased by 0.85 km² in
390 area whereas the areas of unconnected-glacier-fed and non-glacier-fed lakes remained stable
391 as a result of disconnections from glaciers (Figure 7).

392 In the GLCS2, end moraine-dammed lakes increased by 2.48 km² and contributed most of
393 the glacier lake area expansion, whereas supraglacial, ice-blocked and later moraine-dammed
394 lakes decreased slightly in both number and area. Glacial erosion lakes accounted for the
395 maximum percentage (about 66% for both count and area) in each time period and remained
396 stable (Figure 8).

397 Spatially, glacial lake changes in number and area vary among different mountain ranges
398 and basins between 1990 and 2020 in the study area. Glacial lakes across the west Himalaya
399 and Hindu Kush increased both in number and area between 1990 and 2020 whereas the total
400 number of glacial lakes decreased in the Karakoram, Pamir and Tien Shan of study area
401 (Table 4). The total area of glacial lakes continued to increase in the Hindu Kush, but
402 decreased between 1990 and 2000 and increased between 2000 and 2020 in the Himalaya.
403 The total number of glacial lakes continuously decreased in the Pamir and Tien Shan in the
404 past three decades but increased at the first stage and decreased after in the Karakoram. The
405 total area of glacial lakes persistently grew in the Pamir whereas fluctuated in the Tien Shan
406 and Karakoram.

407 The total numbers of glacial lakes in Shingo, Shigar and Shyok basins were stable (Figure
408 9a and b); however, the areal changes were less so, including being stable for Shingo,
409 decreasing for Shigar, and increasing for Shyok. The total number of glacial lakes increased
410 in the basins of Astor, Gilgit and Taxkorgan, whereas the total area of glacial lakes remained
411 stable in Astor and Gilgit basins and decreased in Taxkorgan basin. The total numbers of
412 Kashgar and Hunza basins decreased, whereas the total area of glacial lakes remained stable
413 in Kashgar and increased in the Hunza basin.

414

415 **Table 4.** Distributions in count and area (km²) of glacial lakes among mountain ranges within the study area.

Source and year	Tien Shan	Karakoram	Pamir	Hindu Kush	Himalaya	Total
Landsat in 1990	10 (0.12)	370 (11.11)	178 (13.73)	780 (28.33)	816 (31.81)	2154 (85.10)
Landsat in 2000	7 (0.11)	393 (11.76)	163 (13.96)	792 (28.50)	829 (31.77)	2184 (86.10)
Landsat in 2020	5 (0.17)	334 (10.10)	182 (14.14)	835 (29.25)	878 (32.65)	2234 (86.31)
Sentinel in 2020*	11 (0.21)	479 (11.69)	262 (15.71)	880 (34.96)	959 (33.39)	2591 (95.96)

416 *Note: Glacial lake greater than 4500 m² are calculated for Sentinel-2 derived dataset in order to be in line with Landsat
417 derived dataset.

418 5.2 Glacier lake distribution observed from Sentinel-2

419 Sentinel-derived results shows that there are 7,560 glacial lakes (103.70±8.45 km²) in 2020
420 across the entire CPEC (Table 5) under a minimum mapping unit of 5 pixels (500 m²).

421 Similar to the pattern from Landsat mapping, the lake abundance extracted from Sentinel
422 images is inversely related to lake size (following a typical Pareto distribution). The smallest
423 size class (0.0005-0.0045 km²) contains the maximum lake count (4,969) but the least lake



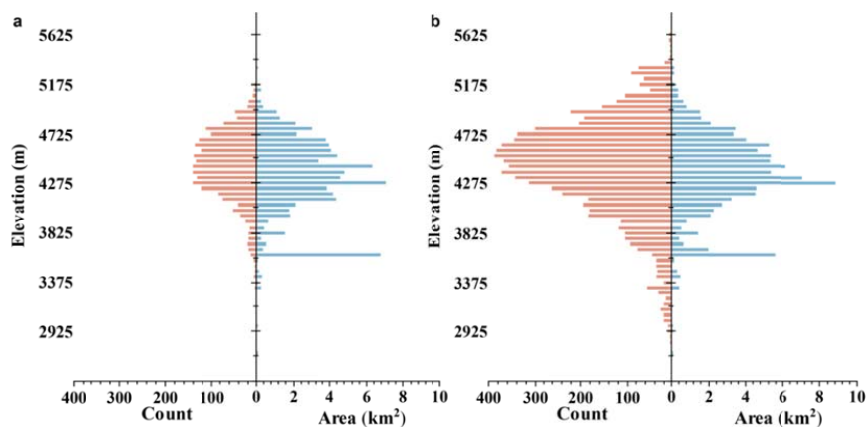
424 area ($7.73 \pm 2.62 \text{ km}^2$) (Table 5), which is not available in the Landsat-derived lake data due to
 425 a coarser spatial resolution. In each size class, there are also a higher number of larger glacial
 426 lakes from Sentinel than that from Landsat images. The discrepancy is mainly attributed to
 427 inconsistency of image acquisition dates and spatial resolutions.

428
 429 **Table 5.** Count and area of glacial lakes mapped from Sentinel and Landsat images in 2020 between
 430 various size classes

Lake size km ²	Glacial lakes from Sentinel count (km ²)	Glacial lakes from Landsat count (km ²)	Overlap % (%)
0.0005-0.0045	4969 (7.73 ± 2.62)	—	—
0.0045-0.05	2182 (35.52 ± 3.72)	1870 (31.47 ± 9.57)	85.70 (88.60)
0.05-0.1	237 (16.37 ± 0.89)	204 (14.07 ± 2.18)	86.08 (85.95)
0.1-0.2	122 (16.88 ± 0.68)	115 (15.91 ± 1.83)	94.26 (94.25)
≥ 0.2	50 (27.20 ± 0.54)	45 (24.86 ± 1.40)	90.00 (91.40)
Total	7560 (103.70 ± 8.45)	2234 (86.31 ± 14.98)	—

431
 432 Compared with our Landsat-based product, glacial lakes from Sentinel-2 have similar
 433 distribution characteristics (Figure 9c and d) among mountain ranges, basins, types and
 434 altitudinal locations (Figure 10); meanwhile, a larger quantity of glacier lakes, with more
 435 accurate boundaries and a greater total lake area, were generated from Sentinel-2 images.
 436 Taking altitudinal distribution for example, the number and size of glacial lakes in the study
 437 area appear follow a normal distribution against elevation for both Sentinel-2 and Landsat
 438 derived products (Figure 10). The elevation of all glacial lakes mapped in 2020 based on
 439 Sentinel-2 images ranged from 2500 m to 5750 m (a.s.l.), with 89.58% between 3600 m and
 440 5100 m and a mean altitude of 4421 m. The peak number appears between 4500 m and 4550
 441 m whereas the maximum area emerges between 4250 m and 4300 m. The anomalously large
 442 area between 3600 and 3650 m shows up in Fig. 10b because of several disproportionately
 443 large lakes. Although Landsat derived lakes show a similar distribution pattern to Sentinel
 444 derived lakes, the lake count and area in each altitudinal band are greater in the Sentinel
 445 product due to the improved spatial resolution and image quality.

446



447

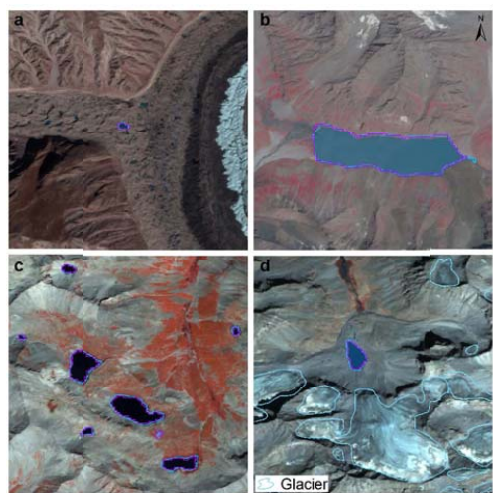
448 **Figure 10.** Altitudinal distribution of glacial lakes in 2020 derived from Landsat (a) and Sentinel images
449 (b)

450

451 6 Discussions

452 6.1 Comparison of Sentinel-2 and Landsat derived products

453 Glacial lakes from Landsat and Sentinel images have a high consistency in number and area
454 with overlap rates from 85.7% to 94.26% for all lakes greater than 0.0045 km² approximately
455 (Table 5), implying a good potential for coordinated utility with Landsat archived observation
456 (Figure 11). Lake extents extracted from Landsat and Sentinel images match well for various
457 types and sizes (Table 4). The best consistency rate reaches 94% for the glacial lakes between
458 0.1 km² and 0.2 km². The difference in area of glacial lakes extracted from Landsat and
459 Sentinel images generally lies within the uncertainty ranges.



460

461 **Figure 11.** High consistency of lake extents extracted from Landsat and Sentinel images. Lake types



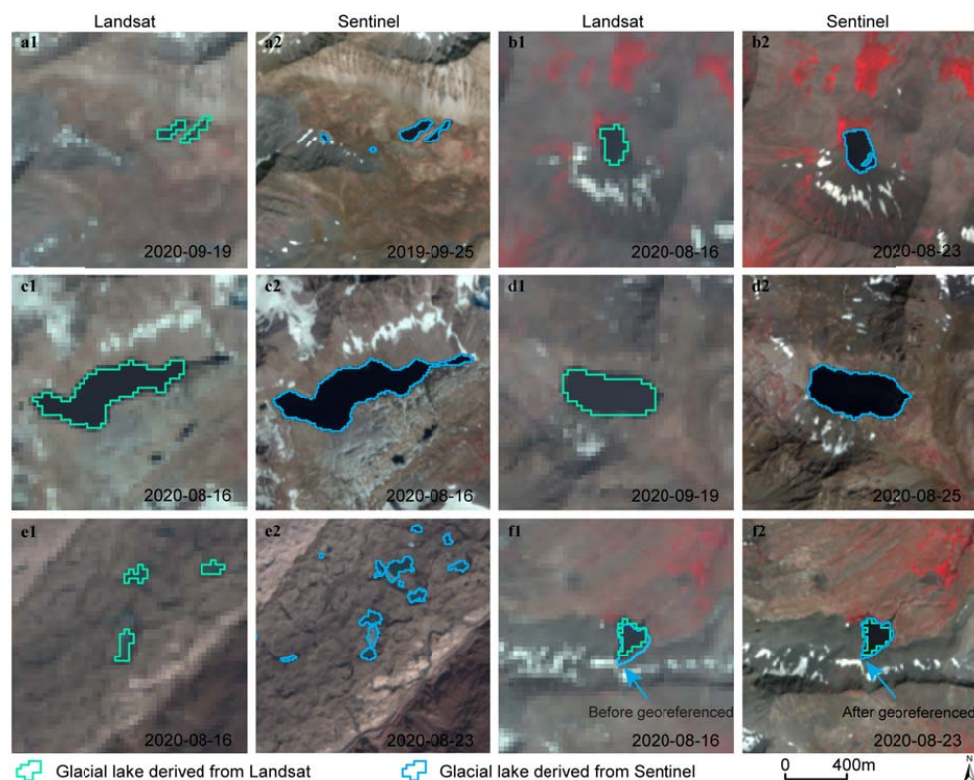
462 shown include supraglacial (a), glacier-fed moraine-dammed (b), unconnected glacial erosion lake without
463 glacier melt supply (c) and glacier-fed moraine-dammed (d).

464

465 Spatial resolution of satellite images plays a primary role in the discrepancies in count and
466 area of glacial lakes extracted from Landsat (30 m) and Sentinel (10 m) observations. Due to
467 a finer spatial resolution, Sentinel images can extract more glacial lakes and more accurate
468 extents than those from Landsat images. We set the same 5 pixels as the minimum mapping
469 unit for both Landsat and Sentinel images, which corresponds to a minimum area of 0.0045
470 km² and 0.0005 km², respectively. The minimum mapping area results in generating nearly
471 5000 more lakes from Sentinel images than from Landsat images, causing the greatest
472 discrepancy in number of the two glacial lake products (Table 5), such as Figure 12a.
473 Meanwhile, Sentinel images are able to depict boundaries of glacial lake with a lower
474 uncertainty (Figure 12b-d). For example, some small islands and narrow channels (Figure 12b
475 and c) were mapped from Sentinel imagery that are unable to be detected in Landsat imagery.

476 Different acquisition dates between Sentinel and Landsat images also contribute to the
477 discrepancy of those two glacial lake datasets. Acquiring same-day images from the two
478 sensors were not always possible due to the impacts of cloud contaminations, topographic
479 shadows, snow cover and revisit periods (Williamson et al., 2018; Paul et al., 2020). Glacial
480 lakes are changing temporally in the context of climate and glacier changes, taking
481 supraglacial lakes for example that evolve dramatically in a short period (Figure 12e). Despite
482 our efforts of leveraging all available high-quality images, the overlap of acquisition dates
483 between Landsat and Sentinel images for the same location is relatively low in this study area,
484 and the consequential temporal gaps led to a difference in the number and area of the derived
485 glacial lakes.

486 Displacement between images also resulted in a certain degree of discrepancy between
487 Landsat and Sentinel derived glacial lakes. All images used in this study have been
488 orthorectified, but we still find that a few Sentinel images were not well matched with
489 Landsat images, leading to the discrepancy between the two glacial lake datasets (Figure 12f).
490 We manually georeferenced the shifted images to minimize the difference between Sentinel
491 and Landsat derived glacial lakes (Figure 12f). Original geo-referencing accuracy is
492 approximate half of one pixel for Landsat and Sentinel image, and this displacement likely
493 contributes a minor error to glacial lake changes at various time periods. Although we could
494 not eliminate this intrinsic error, the error has been considered in the uncertainty assessment
495 of our glacial lake mapping.



496
497 **Figure 12.** Discrepancy of lake extents extracted from Landsat and Sentinel images.
498

499 6.2 Comparison with other datasets

500 Glacial lake datasets play a fundamental role in GLOF risk evaluation, glacier change
501 prediction, and water resource availability. An increasing number of glacial lake datasets
502 have been released over the past years, and most of them were produced from long-term
503 Landsat archives. Glacial lake datasets using Sentinel images are so scarce that we are unable
504 to compare our product with other existing ones in the study area. Here we selected four
505 available glacial lake datasets to compare with our Landsat-derived dataset.

506 Our study provides the latest glacial lake dataset (in 2020) and the most long-term Landsat
507 observation (1990 to 2020) for this study, with a range of critical attributes including two
508 types of classification systems. Within the same study area, our 2020 glacial lakes appear to
509 be closest to the 2018 dataset produced by Wang et al (2020), with the highest overlap of
510 greater than 74% in both number and area (Table 6). In Wang et al. (2020), the minimum
511 mapping unit is 6 pixels so their dataset has a smaller lake quantity. However, their dataset
512 contains all lakes within 10 km of glacier boundaries, including many large
513 landslide-dammed lakes that are excluded in our glacial lake mapping. As a result, their total
514 glacier lake area is greater than ours. The overlapping rates between Wang's glacial lakes
515 (2020) in 1990 and ours are more than 69% in both number and area. However, their results
516 show a distinct increase of glacial lakes in number and area between 1990 and 2018 (Wang et



517 al., 2020) whereas our data show a more stable change between 1990 and 2020. One possible
 518 reason is that manually delineating glacial lakes twice by different operators during Wang's
 519 lake mapping (2020) exacerbates the errors of mapping. Another reason is that their data
 520 contains landslide-dammed lakes that fluctuate greatly with time and expanded recently. One
 521 example is the Attabad Lake (Located at 36°18'22.33"N, 74°49'34.36"E).

522
 523 **Table 6.** Comparison of different glacial lake datasets sourced from Landsat images in the study area.

Acquisition year (period)	Method	MMU m ² (pixels)	Count (km ²)	Overlap % (%)	Reference
1990 (1988-1993)	Manual	5400 (6)	1720 (89.68±13.69)	69.17 (76.33)	Wang et al., 2020
1990 (1990-1999)	Automated	50000 (55)	145 (20.28)	6.27 (21.66)	Shugar et al., 2020
1990 (1989-1992)	Manual	2700 (3)	622 (51.93±10.15)	27.72 (39.94)	Zhang et al., 2015
1990 (1989-1994)	Automated & Manual	4500 (5)	2154 (85.10±14.66)	—	This study
2000 (1999-2001)	Manual	2700 (3)	724 (61.41±11.91)	31.91 (46.97)	Zhang et al., 2015
2000 (2000-2004)	Automated	50000 (55)	155 (22.35)	6.78 (23.72)	Shugar et al., 2020
2008	Automated & Manual	8100 (9)	1067 (65.45)	44.14 (53.58)	Chen et al., 2021
2000 (1996-2004)	Automated & Manual	4500 (5)	2184 (86.10±14.83)	—	This study
2018 (2017-2018)	Manual	5400 (6)	1956 (102.46±15.48)	74.57 (85.63)	Wang et al., 2020
2015 (2015-2018)	Automated	50000 (55)	148 (21.45)	6.27 (22.97)	Shugar et al., 2020
2017	Automated & Manual	8100 (9)	1063 (63.23)	45.21 (57.78)	Chen et al., 2021
2020 (2016-2020)	Automated & Manual	4500 (5)	2234 (86.31±14.98)	—	This study

524 Note: MMU represents minimum mapping units.

525
 526 The second highest overlapping rate is approximate 55% in area with Chen's data in 2008
 527 and 2017 (Chen et al., 2021). However, the overlapping rate in number is nearly 45% due to
 528 their larger minimum mapping unit (9 pixels). Similarly, a minimum mapping unit of 55
 529 pixels (50000 m²) in Shugar et al.'s, dataset (2020) led to the lowest overlap with less than 24%
 530 in area. Zhang's dataset shows fewer glacial lakes in 1990 and 2000 even with a smaller
 531 minimum mapping unit of 3 pixels (Zhang et al., 2015). By inspecting their dataset, we
 532 attributed this anomalous discrepancy to a range of glacial lakes that were missed during their
 533 manual delineation as a result of insufficient high quality images in the earlier Landsat era.
 534 Our Landsat derived glacial lake dataset has been visually cross-checked over three time
 535 periods after the step of object-based automated lake mapping, and also been visually
 536 validated by Sentinel-2 derived glacial lakes. Through this series of quality assurance, we aim
 537 at delivering one of the most reliable multi-decadal glacial lake products for this study area.

538 Other factors, such as minimum mapping units, definition of glacial lakes and study areas,
 539 image quality and acquisition dates, mapping methods and quality assurance workflow, might
 540 also lead to the discrepancies between the glacial lake datasets. Despite such discrepancies,
 541 an increasing number of publically-shared datasets benefit potential users to select the most
 542 suitable one for their objectives. Herein, we provide an up-to-date glacial lake dataset derived
 543 from both Landsat and Sentinel observations, which further promoted the capacity of GLOFs
 544 risk assessment and predicting glacier evolutions in the context of climate change.



545 6.3 Limitation and updating plan

546 We would like to acknowledge several limitations of our glacier lake dataset, largely due the
547 availability of high quality satellite images in the study area and inadequate field survey data
548 (Wang et al., 2020; Chen et al., 2021). First, it is unlikely to collect enough good-quality
549 images within one calendar year for the entire study area due to high possibility of cloud or
550 snow covers. Even though an capacity of repetitive observations for Landsat8 OLI and
551 Sentinel-2 increased (Williamson et al., 2018; Paul et al., 2020; Roy et al., 2014; Wulder et
552 al., 2019), the 2020 glacial lake dataset has to employ images acquired in other years besides
553 2020. Most images used from Landsat and Sentinel platforms were imaged in autumn, and
554 some images taken between April and July and in November also were employed.
555 Distribution and changes in glacial lakes primarily represent the characteristics between
556 August and October. Glacial lakes evolve with time and space (Nie et al., 2017), and subtle
557 inter- and intra-annual changes (Liu et al., 2020) in glacial lake dataset of each time period
558 were ignored. Second, field investigation data are limited due to low accessibility of high
559 mountain environment in the study area, which restrained the accuracy in classifying the
560 glacial lake types. Although very high-resolution Google Earth images were utilized to assist
561 in lake type interpretation, occasional misclassification was inevitable. We implemented two
562 types of classification systems based on a careful utilization of glacier data, DEM,
563 geomorphological features and expert knowledge. However, the lack of in situ survey
564 prohibited a thorough validation of the glacial lake types.

565 7 Data availability

566 Our glacial lake dataset extracted from Sentinel-2 images in 2020 and Landsat observation
567 between 1990 and 2020 are available online via the Mountain Science Data Center, the
568 Institute of Mountain Hazards and Environment, the Chinese Academy of Sciences at
569 <https://doi.org/10.12380/Glaci.msdc.000001> (Lesi et al., 2022). The glacial lake dataset is
570 provided in both ESRI shapefile format (total size of 22.6 MB) and the Geopackage format
571 (version 1.2.1) with a total size of 9.2MB, which can be opened and further processed by
572 open-source geographic information system software such as QGIS. The glacial lake dataset
573 will be updated using newly collected Landsat and Sentinel images at a five-year interval or
574 modified according to user feedbacks. The updated glacial lake dataset will continue to be
575 released freely and publicly on the Mountain Science Data Center sharing platform.

576 8 Conclusions

577 Glacial lake inventories of the entire China-Pakistan Economic Corridor in 2020 were
578 completed based on Landsat and Sentinel-2 images using a human-interactive and
579 semi-automated mapping method. Both Landsat and Sentinel derived glacial lake datasets
580 show similar characteristics in spatial distribution and in the statistics of count and area. By
581 contrast, glacial lake dataset derived from Sentinel-2 images with a spatial resolution of 10 m
582 has a lower mapping error and more accurate lake boundary than those from 30 m spatial
583 resolution Landsat images whereas Landsat imagery is more suitable to analyze
584 spatial-temporal changes at longer time scale due to its long-term archived observation at a



585 consistent spatial resolution of 30 m started from around 1990.
586 Glacial lakes in the study area remain relatively stable with a slight increase in number and
587 area between 1990 and 2020 according to Landsat observations. Our dataset reveals that 2154
588 glacial lakes in 1990 covering $85.1 \pm 14.66\text{km}^2$ increased to 2234 lakes with a total area of
589 $86.31 \pm 14.98\text{km}^2$. The same mapping method and rigorous workflow of quality assurance
590 and quality control used in this study reduced the error in multi-temporal changes of glacial
591 lakes.

592 The Hanshaw's error estimation method for automated lake mapping was improved by
593 removing repeatedly calculated edge pixels that vary with lake shape. Therefore, the newly
594 proposed method reduces the estimated value of uncertainty from satellite observations.

595 Our glacial lake dataset contains a range of critical parameters that maximize their
596 potential utility for GLOFs risk evaluation and glacier-lake evolution projection. The dual
597 classification systems of glacial lake types were developed and are very likely to attract
598 broader researchers and scientists to use our datasets. In comparison with other existing
599 glacial lake datasets, our products were created through a thorough consideration of lake
600 types, cross checks and rigorous quality assurance, and will be updated and released
601 continuously in the data center of mountain science. As such, we expect that our glacial lake
602 dataset will have significant values for cryospheric-hydrology research, assessment of
603 glacier-related hazards and engineering project construction in the CPEC.

604

605 **Supplement.** The supplement related to this article is available online.

606

607 **Author contributions.** ML and YN conceived the study, ML, YN and XD performed data
608 processing and analysis of the glacial lake inventory data, JW contributed to tool development
609 and mapping methods, ML and YN wrote the manuscript. All authors reviewed and edited the
610 manuscript before submission.

611

612 **Competing interests.** The authors declare no conflict of interest.

613

614 **Acknowledgements.**

615 This study was supported by the National Natural Science Foundation of China (Grant Nos.
616 42171086, 41971153), the International Science & Technology Cooperation Program of
617 China (No. 2018YFE0100100), the Chinese Academy of Sciences "Light of West China" and
618 Natural Sciences and Engineering Research Council of Canada (Grant No. DG-2020-04207).

619

620

621

622 **References**

623 Ashraf, A., Naz, R., Iqbal, M.B.: Altitudinal dynamics of glacial lakes under changing climate in the Hindu

624 Kush, Karakoram, and Himalaya ranges. *Geomorphology*, 283: 72-79,

625 <https://doi.org/10.1016/j.geomorph.2017.01.033>, 2017.



- 626 Azam, M.F., Kargel, J.S., Shea, J.M., Nepal, S., Haritashya, U.K., Srivastava, S., Maussion, F., Qazi, N.,
627 Chevallier, P., Dimri, A.P., Kulkarni, A.V., Cogley, J.G., Bahuguna, I.: Glaciohydrology of the
628 Himalaya-Karakoram. *Science*, 373: eabf3668, <https://doi.org/10.1126/science.abf3668>, 2021.
- 629 Battamo, A.Y., Varis, O., Sun, P., Yang, Y., Oba, B.T., Zhao, L.: Mapping socio-ecological resilience along the
630 seven economic corridors of the Belt and Road Initiative. *J. Clean. Prod.*, 309: 127341,
631 <https://doi.org/10.1016/j.jclepro.2021.127341>, 2021.
- 632 Bhambri, R., Hewitt, K., Kawishwar, P., Kumar, A., Verma, A., Snehmani, Tiwari, S., Misra, A.: Ice-dams,
633 outburst floods, and movement heterogeneity of glaciers, Karakoram. *Global Planet. Change*, 180: 100-116,
634 <https://doi.org/10.1016/j.gloplacha.2019.05.004>, 2019.
- 635 Bhattacharya, A., Bolch, T., Mukherjee, K., King, O., Menounos, B., Kapitsa, V., Neckel, N., Yang, W., Yao, T.:
636 High Mountain Asian glacier response to climate revealed by multi-temporal satellite observations since the
637 1960s. *Nat. Commun.*, 12: 4133, <https://doi.org/10.1038/s41467-021-24180-y>, 2021.
- 638 Bolch, T., Pieczonka, T., Mukherjee, K., Shea, J.: Brief communication: Glaciers in the Hunza catchment
639 (Karakoram) have been nearly in balance since the 1970s. *The Cryosphere*, 11: 531-539,
640 <https://doi.org/10.5194/tc-11-531-2017>, 2017.
- 641 Brun, F., Berthier, E., Wagnon, P., Käab, A., Treichler, D.: A spatially resolved estimate of High Mountain Asia
642 glacier mass balances from 2000 to 2016. *Nat. Geosci.*, 10: 668-673, <https://doi.org/10.1038/ngeo2999>, 2017.
- 643 Brun, F., Wagnon, P., Berthier, E., Jomelli, V., Maharjan, S.B., Shrestha, F., Kraaijenbrink, P.D.A.:
644 Heterogeneous Influence of Glacier Morphology on the Mass Balance Variability in High Mountain Asia. *J.*
645 *Geophys. Res-Earth*, 124: 1331-1345, <https://doi.org/10.1029/2018JF004838>, 2019.
- 646 Chen, F., Zhang, M., Guo, H., Allen, S., Kargel, J.S., Haritashya, U.K., Watson, C.S.: Annual 30 m dataset for
647 glacial lakes in High Mountain Asia from 2008 to 2017. *Earth System Science Data*, 13: 741-766,



- 648 <https://doi.org/10.5194/essd-13-741-2021>, 2021.
- 649 Chen, X., Cui, P., You, Y., Cheng, Z., Khan, A., Ye, C., Zhang, S.: Dam-break risk analysis of the Attabad
650 landslide dam in Pakistan and emergency countermeasures. *Landslides*, 14: 675-683,
651 <https://doi.org/10.1007/s10346-016-0721-7>, 2017.
- 652 Emmer, A., Cuřin, V.: Can a dam type of an alpine lake be derived from lake geometry? A negative result. *J. Mt.
653 Sci.-Engl.*, 18: 614-621, <https://doi.org/10.1007/s11629-020-6003-9>, 2021.
- 654 Farr, T.G., Rosen, P.A., Caro, E., Crippen, R., Duren, R., Hensley, S., Kobrick, M., Paller, M., Rodriguez, E.,
655 Roth, L., Seal, D., Shaffer, S., Shimada, J., Umland, J., Werner, M., Oskin, M., Burbank, D., Alsdorf, D.: The
656 Shuttle Radar Topography Mission. *Rev. Geophys.*, 45: RG2004, <https://doi.org/10.1029/2005RG000183>, 2007.
- 657 Gardelle, J., Arnaud, Y., Berthier, E.: Contrasted evolution of glacial lakes along the Hindu Kush Himalaya
658 mountain range between 1990 and 2009. *Global Planet. Change*, 75: 47-55,
659 <https://doi.org/10.1016/j.gloplacha.2010.10.003>, 2011.
- 660 Hanshaw, M.N., Bookhagen, B.: Glacial areas, lake areas, and snow lines from 1975 to 2012: status of the
661 Cordillera Vilcanota, including the Quelccaya Ice Cap, northern central Andes, Peru. *The Cryosphere*, 8:
662 359-376, <https://doi.org/10.5194/tc-8-359-2014>, 2014.
- 663 Hewitt, K.: The Karakoram Anomaly? Glacier Expansion and the ‘Elevation Effect,’ Karakoram Himalaya. *Mt.
664 Res. Dev.*, 25: 332-340, [https://doi.org/10.1659/0276-4741\(2005\)025\[0332:TKAGEA\]2.0.CO;2](https://doi.org/10.1659/0276-4741(2005)025[0332:TKAGEA]2.0.CO;2), 2005.
- 665 Hewitt, K., 2014. *Glaciers of the Karakoram Himalaya: Glacial Environments, Processes, Hazards and
666 Resources*. Springer, Dordrecht.
- 667 Huggel, C., Käab, A., Haeberli, W., Teyssie, P., Paul, F.: Remote sensing based assessment of hazards from
668 glacier lake outbursts: a case study in the Swiss Alps. *Can. Geotech. J.*, 39: 316-330,
669 <https://doi.org/10.1139/t01-099>, 2002.



- 670 Hugonnet, R., McNabb, R., Berthier, E., Menounos, B., Nuth, C., Girod, L., Farinotti, D., Huss, M., Dussailant,
671 I., Brun, F., Kääb, A.: Accelerated global glacier mass loss in the early twenty-first century. *Nature*, 592:
672 726-731, <https://doi.org/10.1038/s41586-021-03436-z>, 2021.
- 673 Jarvis, A., Reuter, H.I., Nelson, A., Guevara, E., 2008. Hole-filled seamless SRTM data V4. 2008, International
674 Centre for Tropical Agriculture (CIAT), available from <http://srtm.csi.cgiar.org>.
- 675 Jiang, S., Nie, Y., Liu, Q., Wang, J., Liu, L., Hassan, J., Liu, X., Xu, X.: Glacier Change, Supraglacial Debris
676 Expansion and Glacial Lake Evolution in the Gyirong River Basin, Central Himalayas, between 1988 and 2015.
677 *Remote Sens.-Basel*, 10: 986, <https://doi.org/10.3390/rs10070986>, 2018.
- 678 Kääb, A., Berthier, E., Nuth, C., Gardelle, J., Arnaud, Y.: Contrasting patterns of early twenty-first-century
679 glacier mass change in the Himalayas. *Nature*, 488: 495-498, <https://doi.org/10.1038/nature11324>, 2012.
- 680 Lesi, M., Nie, Y., Shugar, D.H., Wang, J., Deng, Q., Chen, H.: Landsat and Sentinel-derived glacial lake dataset
681 in the China-Pakistan Economic Corridor from 1990 to 2020. Mountain Science Data Center,
682 <https://doi.org/10.12380/Glaci.msdc.000001>, 2022.
- 683 Li, Z., Deng, X., Zhang, Y.: Evaluation and convergence analysis of socio-economic vulnerability to natural
684 hazards of Belt and Road Initiative countries. *J. Clean. Prod.*, 282: 125406,
685 <https://doi.org/10.1016/j.jclepro.2020.125406>, 2021.
- 686 Liu, Q., Mayer, C., Wang, X., Nie, Y., Wu, K., Wei, J., Liu, S.: Interannual flow dynamics driven by frontal
687 retreat of a lake-terminating glacier in the Chinese Central Himalaya. *Earth Planet. Sc. Lett.*, 546: 116450,
688 <https://doi.org/10.1016/j.epsl.2020.116450>, 2020.
- 689 Lutz, A.F., Immerzeel, W.W., Shrestha, A.B., Bierkens, M.F.P.: Consistent increase in High Asia's runoff due to
690 increasing glacier melt and precipitation. *Nat. Clim. Change*, 4: 587-592, <https://doi.org/10.1038/nclimate2237>,
691 2014.



- 692 Lyons, E.A., Sheng, Y., Smith, L.C., Li, J., Hinkel, K.M., Lenters, J.D., Wang, J.: Quantifying sources of error
693 in multitemporal multisensor lake mapping. *Int. J. Remote Sens.*, 34: 7887-7905,
694 <https://doi.org/10.1080/01431161.2013.827343>, 2013.
- 695 Martín, C.N.S., Ponce, J.F., Montes, A., Balocchi, L.D., Gorza, C., Andrea, C.: Proglacial landform assemblage
696 in a rapidly retreating cirque glacier due to temperature increase since 1970, Fuegian Andes, Argentina.
697 *Geomorphology*, 390: 107861, <https://doi.org/10.1016/j.geomorph.2021.107861>, 2021.
- 698 Maurer, J.M., Schaefer, J.M., Rupper, S., Corley, A.: Acceleration of ice loss across the Himalayas over the past
699 40 years. *Sci. Adv.*, 5: eaav7266, <https://doi.org/10.1126/sciadv.aav7266>, 2019.
- 700 Mcfeeters, S.K.: The use of the Normalized Difference Water Index (NDWI) in the delineation of open water
701 features. *Int. J. Remote Sens.*, 17: 1425 - 1432 1996.
- 702 Nie, Y., Zhang, Y., Liu, L., Zhang, J.: Glacial change in the vicinity of Mt. Qomolangma (Everest), central high
703 Himalayas since 1976. *J. Geogr. Sci.*, 20: 667-686, <https://doi.org/10.1007/s11442-010-0803-8>, 2010.
- 704 Nie, Y., Sheng, Y., Liu, Q., Liu, L., Liu, S., Zhang, Y., Song, C.: A regional-scale assessment of Himalayan
705 glacial lake changes using satellite observations from 1990 to 2015. *Remote Sens. Environ.*, 189: 1-13,
706 <https://doi.org/10.1016/j.rse.2016.11.008>, 2017.
- 707 Nie, Y., Liu, Q., Wang, J., Zhang, Y., Sheng, Y., Liu, S.: An inventory of historical glacial lake outburst floods
708 in the Himalayas based on remote sensing observations and geomorphological analysis. *Geomorphology*, 308:
709 91-106, <https://doi.org/10.1016/j.geomorph.2018.02.002>, 2018.
- 710 Nie, Y., Liu, W., Liu, Q., Hu, X., Westoby, M.J.: Reconstructing the Chongbaxia Tsho glacial lake outburst
711 flood in the Eastern Himalaya: Evolution, process and impacts. *Geomorphology*, 370: 107393,
712 <https://doi.org/10.1016/j.geomorph.2020.107393>, 2020.
- 713 Nie, Y., Pritchard, H.D., Liu, Q., Hennig, T., Wang, W., Wang, X., Liu, S., Nepal, S., Samyn, D., Hewitt, K.,



- 714 Chen, X.: Glacial change and hydrological implications in the Himalaya and Karakoram. *Nature Reviews Earth*
715 & Environment, 2: 91-106, <https://doi.org/10.1038/s43017-020-00124-w>, 2021.
- 716 Paul, F., Rastner, P., Azzoni, R.S., Diolaiuti, G., Fugazza, D., Le Bris, R., Nemeč, J., Rabatel, A., Ramusovic,
717 M., Schwaizer, G., Smiraglia, C.: Glacier shrinkage in the Alps continues unabated as revealed by a new glacier
718 inventory from Sentinel-2. *Earth System Science Data*, 12: 1805-1821,
719 <https://doi.org/10.5194/essd-12-1805-2020>, 2020.
- 720 Pfeffer, W.T., Arendt, A.A., Bliss, A., Bolch, T., Cogley, J.G., Gardner, A.S., Hagen, J., Hock, R., Kaser, G.,
721 Kienholz, C., Miles, E.S., Moholdt, G., Mölg, N., Paul, F., Radić, V., Rastner, P., Raup, B.H., Rich, J., Sharp,
722 M.J.: The Randolph Glacier Inventory: a globally complete inventory of glaciers. *J. Glaciol.*, 60: 537-552,
723 <https://doi.org/10.3189/2014JoG13J176>, 2014.
- 724 Post, A., Mayo, L.R., 1971. Glacier dammed lakes and outburst floods in Alaska: U.S. Geological Survey
725 Hydrologic Investigations Atlas 455, U.S. Geological Survey.
- 726 Pritchard, H.D.: Asia's shrinking glaciers protect large populations from drought stress. *Nature*, 569: 649-654,
727 <https://doi.org/10.1038/s41586-019-1240-1>, 2019.
- 728 Quincey, D.J., Richardson, S.D., Luckman, A., Lucas, R.M., Reynolds, J.M., Hambrey, M.J., Glasser, N.F.:
729 Early recognition of glacial lake hazards in the Himalaya using remote sensing datasets. *Global Planet. Change*,
730 56: 137-152, <https://doi.org/10.1016/j.gloplacha.2006.07.013>, 2007.
- 731 Rabus, B., Eineder, M., Roth, A., Bamler, R.: The shuttle radar topography mission—a new class of digital
732 elevation models acquired by spaceborne radar. *ISPRS J. Photogramm.*, 57: 241-262,
733 [https://doi.org/10.1016/S0924-2716\(02\)00124-7](https://doi.org/10.1016/S0924-2716(02)00124-7), 2003.
- 734 RGI Consortium: Randolph Glacier Inventory – A Dataset of Global Glacier Outlines: Version 6.0: Technical
735 Report, <https://doi.org/10.7265/N5-RGI-60>, 2017.



- 736 Rounce, D.R., Hock, R., Shean, D.E.: Glacier Mass Change in High Mountain Asia Through 2100 Using the
737 Open-Source Python Glacier Evolution Model (PyGEM). *Front. Earth Sci*, 7: 331,
738 <https://doi.org/10.3389/feart.2019.00331>, 2020.
- 739 Roy, D.P., Wulder, M.A., Loveland, T.R., C. E., W., Allen, R.G., Anderson, M.C., Helder, D., Irons, J.R.,
740 Johnson, D.M., Kennedy, R., Scambos, T.A., Schaaf, C.B., Schott, J.R., Sheng, Y., Vermote, E.F., Belward,
741 A.S., Bindschadler, R., Cohen, W.B., Gao, F., Hipple, J.D., Hostert, P., Huntington, J., Justice, C.O., Kilic, A.,
742 Kovalsky, V., Lee, Z.P., Lyburner, L., Masek, J.G., Mccorkel, J., Shuai, Y., Trezza, R., Vogelmann, J.,
743 Wynne, R.H., Zhu, Z.: Landsat-8: Science and product vision for terrestrial global change research. *Remote*
744 *Sens. Environ.*, 145: 154-172, <https://doi.org/10.1016/j.rse.2014.02.001>, 2014.
- 745 Sakai, A.: Brief communication: Updated GAMDAM glacier inventory over high-mountain Asia. *The*
746 *Cryosphere*, 13: 2043-2049, <https://doi.org/10.5194/tc-13-2043-2019>, 2019.
- 747 Shean, D.E., Bhushan, S., Montesano, P., Rounce, D.R., Arendt, A., Osmanoglu, B.: A Systematic, Regional
748 Assessment of High Mountain Asia Glacier Mass Balance. *Front. Earth Sci*, 7: 363,
749 <https://doi.org/10.3389/feart.2019.00363>, 2020.
- 750 Sheng, Y., Song, C., Wang, J., Lyons, E.A., Knox, B.R., Cox, J.S., Gao, F.: Representative lake water extent
751 mapping at continental scales using multi-temporal Landsat-8 imagery. *Remote Sens. Environ.*, 185: 129-141,
752 <https://doi.org/10.1016/j.rse.2015.12.041>, 2016.
- 753 Shugar, D.H., Burr, A., Haritashya, U.K., Kargel, J.S., Watson, C.S., Kennedy, M.C., Bevington, A.R., Betts,
754 R.A., Harrison, S., Strattman, K.: Rapid worldwide growth of glacial lakes since 1990. *Nat. Clim. Change*, 10:
755 939-945, <https://doi.org/10.1038/s41558-020-0855-4>, 2020.
- 756 Shugar, D.H., Jacquemart, M., Shean, D., Bhushan, S., Upadhyay, K., Sattar, A., Schwanghart, W., McBride, S.,
757 de Vries, M., Mergili, M., Emmer, A., Deschamps-Berger, C., McDonnell, M., Bhabri, R., Allen, S., Berthier,



758 E., Carrivick, J.L., Clague, J.J., Dokukin, M., Dunning, S.A., Frey, H., Gascoin, S., Haritashya, U.K., Huggel,
759 C., Kaab, A., Kargel, J.S., Kavanaugh, J.L., Lacroix, P., Petley, D., Rupper, S., Azam, M.F., Cook, S.J., Dimri,
760 A.P., Eriksson, M., Farinotti, D., Fiddes, J., Gnyawali, K.R., Harrison, S., Jha, M., Koppes, M., Kumar, A.,
761 Leinss, S., Majeed, U., Mal, S., Muhuri, A., Noetzli, J., Paul, F., Rashid, I., Sain, K., Steiner, J., Ugalde, F.,
762 Watson, C.S., Westoby, M.J.: A massive rock and ice avalanche caused the 2021 disaster at Chamoli, Indian
763 Himalaya. *Science*, 373: 300-306, <https://doi.org/10.1126/science.abh4455>, 2021.
764 Ullah, S., You, Q., Ali, A., Ullah, W., Jan, M.A., Zhang, Y., Xie, W., Xie, X.: Observed changes in maximum
765 and minimum temperatures over China- Pakistan economic corridor during 1980–2016. *Atmos. Res.*, 216:
766 37-51, <https://doi.org/10.1016/j.atmosres.2018.09.020>, 2019.
767 Viviroli, D., Kumm, M., Meybeck, M., Kallio, M., Wada, Y.: Increasing dependence of lowland populations
768 on mountain water resources. *Nature Sustainability*, 3: 917-928, <https://doi.org/10.1038/s41893-020-0559-9>,
769 2020.
770 Wang, J., Sheng, Y., Hinkel, K.M., Lyons, E.A.: Drained thaw lake basin recovery on the western Arctic
771 Coastal Plain of Alaska using high-resolution digital elevation models and remote sensing imagery. *Remote*
772 *Sens. Environ.*, 119: 325-336, <https://doi.org/10.1016/j.rse.2011.10.027>, 2012.
773 Wang, J., Sheng, Y., Tong, T.S.D.: Monitoring decadal lake dynamics across the Yangtze Basin downstream of
774 Three Gorges Dam. *Remote Sens. Environ.*, 152: 251-269, <https://doi.org/10.1016/j.rse.2014.06.004>, 2014.
775 Wang, J., Sheng, Y., Wada, Y.: Little impact of the Three Gorges Dam on recent decadal lake decline across
776 China's Yangtze Plain. *Water Resour. Res.*, 53: 3854-3877, <https://doi.org/10.1002/2016WR019817>, 2017.
777 Wang, J., Song, C., Reager, J.T., Yao, F., Famiglietti, J.S., Sheng, Y., Macdonald, G.M., Brun, F., Schmied,
778 H.M., Marston, R.A., Wada, Y.: Recent global decline in endorheic basin water storages. *Nat. Geosci.*, 11:
779 926-932, <https://doi.org/10.1038/s41561-018-0265-7>, 2018.



- 780 Wang, X., Ding, Y., Liu, S., Jiang, L., Wu, K., Jiang, Z., Guo, W.: Changes of glacial lakes and implications in
781 Tian Shan, Central Asia, based on remote sensing data from 1990 to 2010. *Environ. Res. Lett.*, 8: 44052,
782 <https://doi.org/10.1088/1748-9326/8/4/044052>, 2013.
- 783 Wang, X., Liu, S., Zhang, J.: A new look at roles of the cryosphere in sustainable development. *Advances in*
784 *Climate Change Research*, 10: 124-131, <https://doi.org/10.1016/j.accre.2019.06.005>, 2019.
- 785 Wang, X., Guo, X., Yang, C., Liu, Q., Wei, J., Zhang, Y., Liu, S., Zhang, Y., Jiang, Z., Tang, Z.: Glacial lake
786 inventory of high-mountain Asia in 1990 and 2018 derived from Landsat images. *Earth System Science Data*,
787 12: 2169-2182, <https://doi.org/10.5194/essd-12-2169-2020>, 2020.
- 788 Westoby, M.J., Glasser, N.F., Brasington, J., Hambrey, M.J., Quincey, D.J., Reynolds, J.M.: Modelling outburst
789 floods from moraine-dammed glacial lakes. *Earth-Sci. Rev.*, 134: 137-159,
790 <https://doi.org/10.1016/j.earscirev.2014.03.009>, 2014.
- 791 Williamson, A.G., Banwell, A.F., Willis, I.C., Arnold, N.S.: Dual-satellite (Sentinel-2 and Landsat 8) remote
792 sensing of supraglacial lakes in Greenland. *The Cryosphere*, 12: 3045-3065,
793 <https://doi.org/10.5194/tc-12-3045-2018>, 2018.
- 794 Wulder, M.A., Loveland, T.R., Roy, D.P., Crawford, C.J., Masek, J.G., Woodcock, C.E., Allen, R.G., Anderson,
795 M.C., Belward, A.S., Cohen, W.B., Dwyer, J., Erb, A., Gao, F., Griffiths, P., Helder, D., Hermosilla, T., Hipple,
796 J.D., Hostert, P., Hughes, M.J., Huntington, J., Johnson, D.M., Kennedy, R., Kilic, A., Li, Z., Lymburner, L.,
797 Mccorkel, J., Pahlevan, N., Scambos, T.A., Schaaf, C., Schott, J.R., Sheng, Y., Storey, J., Vermote, E.,
798 Vogelmann, J., White, J.C., Wynne, R.H., Zhu, Z.: Current status of Landsat program, science, and applications.
799 *Remote Sens. Environ.*, 225: 127-147, <https://doi.org/https://doi.org/10.1016/j.rse.2019.02.015>, 2019.
- 800 Yao, C., Wang, X., Zhao, X., Wei, J., Zhang, Y.: Temporal and Spatial Changes of Glacial Lakes in the
801 China-Pakistan Economic Corridor from 1990 to 2018. *Journal of Glaciology and Geocryology*, 42: 33-42,



- 802 <https://doi.org/https://doi.org/10.7522/j.issn.1000-0240.2020.0009>, 2020.
- 803 Yao, T., Thompson, L., Yang, W., Yu, W.S., Gao, Y., Guo, X.J., Yang, X.X., Duan, K.Q., Zhao, H.B., Xu, B.Q.,
- 804 Pu, J.C., Lu, A.X., Xiang, Y., Kattel, D.B., Joswiak, D.: Different glacier status with atmospheric circulations in
- 805 Tibetan Plateau and surroundings. *Nat. Clim. Change*, 2: 663-667, <https://doi.org/10.1038/NCLIMATE1580>,
- 806 2012.
- 807 Yao, X., Liu, S., Han, L., Sun, M., Zhao, L.: Definition and classification system of glacial lake for inventory
- 808 and hazards study. *J. Geogr. Sci.*, 28: 193-205, <https://doi.org/10.1007/s11442-018-1467-z>, 2018.
- 809 Zhang, G., Yao, T., Xie, H., Wang, W., Yang, W.: An inventory of glacial lakes in the Third Pole region and
- 810 their changes in response to global warming. *Global Planet. Change*, 131: 148-157,
- 811 <https://doi.org/10.1016/j.gloplacha.2015.05.013>, 2015.
- 812 Zhang, M., Chen, F., Tian, B.: An automated method for glacial lake mapping in High Mountain Asia using
- 813 Landsat 8 imagery. *J. Mt. Sci.-Engl.*, 15: 13-24, <https://doi.org/10.1007/s11629-017-4518-5>, 2018.
- 814 Zheng, G., Allen, S.K., Bao, A., Ballesteros-Cánovas, J.A., Huss, M., Zhang, G., Li, J., Yuan, Y., Jiang, L., Yu,
- 815 T., Chen, W., Stoffel, M.: Increasing risk of glacial lake outburst floods from future Third Pole deglaciation. *Nat.*
- 816 *Clim. Change*, 11: 411-417, <https://doi.org/10.1038/s41558-021-01028-3>, 2021.
- 817